# Synthesis of Silver Nanocubes@Cobalt Ferrite/Graphitic Carbon Nitride for Electrochemical Water Splitting

Ausrine Zabielaite *, Olegas Eicher-Lorka, Ramunas Levinas, Dijana Simkunaite, Loreta Tamasauskaite-Tamasiunaite *, Eugenijus Norkus

Posted Date: 1 August 2023

doi: 10.20944/preprints202308.0027.v1

Keywords: graphitic carbon nitride; silver nanocubes; cobalt ferrite; polyol method; hydrogen and oxygen evolution

*Article*

# Synthesis of Silver Nanocubes@Cobalt Ferrite/Graphitic Carbon Nitride for Electrochemical Water Splitting

**Ausrine Zabielaite *, Olegas Eicher-Lorka, Ramunas Levinas, Dijana Simkunaite, Loreta Tamasauskaite-Tamasiunaite * and Eugenijus Norkus**

Center for Physical Sciences and Technology (FTMC), Vilnius, Lithuania; ausrine.zabielaite@ftmc.lt (A.Z.); olegas.eicher-lorka@ftmc.lt (O.E.-L.); ramunas.levinas@ftmc.lt (R.S.); dijana.simkunaite@ftmc.lt (D.S.); loreta.tamasauskaite@ftmc.lt (L.T.-T.); eugenijus.norkus@ftmc.lt (E.N.)

* Correspondence: ausrine.zabielaite@ftmc.lt; loreta.tamasauskaite@ftmc.lt

**Abstract:** This study presents the synthesis of graphitic carbon nitride (g–$C_3N_4$) and its nanostructures with cobalt ferrite oxide ($CoFe_2O_4$) and silver nanocubes (Ag) using the combined pyrolysis of melamine and polyol method. The resulted nanostructures were tested as electrocatalysts for hydrogen and oxygen evolution reactions in alkaline media. It was found that the Ag/$CoFe_2O_4$/g–$C_3N_4$ shows the highest current density and gives the lowest overpotential of −259 mV for HER to reach a current density of 10 mA $cm^{-2}$ in 1 M KOH. Overpotentials to reach the current density of 10 mA·$cm^{-2}$ for OER are 370.2 mV and 382.7 mV for Ag/$CoFe_2O_4$/g–$C_3N_4$ and $CoFe_2O_4$/g–$C_3N_4$, respectively. The above results demonstrate that $CoFe_2O_4$/g–$C_3N_4$ and Ag/$CoFe_2O_4$/g–$C_3N_4$ materials could act as a bifunctional catalyst due to the notable performance towards HER and OER and for total water splitting in practical applications is a promising alternative to noble metal-based electrocatalysts.

**Keywords:** graphitic carbon nitride; silver nanocubes; cobalt ferrite; polyol method; hydrogen and oxygen evolution

## 1. Introduction

The development of green hydrogen production technologies by water electrolysis (water splitting) has become one of the major current priorities [1–6]. The challenge is to design and development novel, non-noble and low-cost bifunctional electrode materials with high efficiency for both HER and OER. Transition-metal boride/phosphide-based materials are attractive catalysts for $H_2$ release due to their advantages of earth-abundant elements, considerable catalytic activity, high stability, and low cost [7]. Metal nanoparticles as catalysts have also attracted much attention over the last decades owing to their unique properties. However, metal nanoparticles tend to aggregate into clumps and ultimately into their bulk counterparts due to their high surface energy, thus leading to decreased catalytic activity and suffering in long-term stability. Dispersing or anchoring the metal nanoparticles onto certain supporting materials with a large surface area to form a supported catalyst can improve the stability of the catalyst by averting the aggregation of nanoparticles. Therefore, selecting suitable supports is crucial in obtaining stable and catalytically active catalysts. So far, many supporting materials (metal oxides, organic polymer, porous materials, carbon-based materials, etc.) have been broadly investigated to stabilize metal nanoparticles. Recently, graphitic carbon nitride (g–$C_3N_4$) has been widely used as a base carrier for the deposition of nanoparticles of various metals (Ni, Co, Mn, Cu, Fe, etc.) and their oxides. g–$C_3N_4$ has excellent properties such as high bulk modulus, good thermal conductivity, small mechanical friction coefficient, high elasticity and chemical inertness. Moreover, g–$C_3N_4$ is also a very promising material that can replace the commonly used carbon for the production of catalysts due its high nitrogen (N) content. The production of this material does not require high costs and is easy to produce. A simple approach to obtain g–C3N4 is polymerization of cyanamide, dicyandiamide or melamine [8–12]. Depending on reaction conditions,

 doi:10.20944/preprints202308.0027.v1



different materials with different degrees of condensation, properties and reactivities can be obtained [8]. In this study, the g–$C_3N_4$ was synthesized using the melamine as a precursor. Figure 1 presents the structure of melamine, which is a kind of three triazine heterocyclic organic compound.

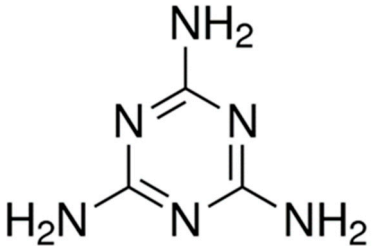

**Figure 1.** Structure of melamine.

Heating the melamine at different temperatures allows to obtain different morphologies of g–$C_3N_4$, ranging from nanosheets to rolled nanosheets, nanotubes, and nanoflakes with nanoparticles, depending on the thermal polymerization temperatures of 500, 520, and 540 °C, respectively [13].

However, optimal use of g–$C_3N_4$ for electrochemical applications requires the improvement of its poor conductivity, which can be increased in several ways: physically mixing g-$C_3N_4$ with conductive carbon materials, immobilizing g-$C_3N_4$ on carbon bases (carriers) or depositing metal nanoparticles using microwave-assisted processes, hydrothermal and solvothermal syntheses routes, sol-gel processes, chemical reduction, etc. The application of earth-abundant transition/noble metals-free (TMs, where M=Co, Ni, Fe, Mn, Mo) and TMs-based alloys or non-metallic (TMXs, where X=N, O, S, C, P, etc.) compounds as active electrocatalysts for HER/OER has been reported [14–18]. TMXs have received much attention due to their distinctive structural features, abundant active sites, tunable electronic properties, compositions, and ease of employment for large-scale production. Co, Ni, and Fe are typically characterized as the most powerful materials for water splitting [19–22]. Among them, Co-based electrocatalysts, including cobalt oxides [23], hydroxides [24], nitrides [25,26], sulfides [27], and selenides [28], phosphides [29], cobalt ferrite oxide [6,30,31], play a rather significant role in water splitting and are widely used in HER/OER [32,33]. However, their catalytic performance and stability do not yet meet the requirements for use in practical applications. Many electrocatalysts based on cobalt suffer from poor electrical conductivity and hence low charge transfer efficiency [32,33]. Efficient and stable Co-based electrocatalytic materials with sufficient intrinsic electronic structure and an unlimited number of active sites on the surface for optimized water splitting remain a challenge.

In this study, we reported the synthesis of cobalt ferrite oxide ($CoFe_2O_4$)@g–$C_3N_4$ and silver nanocubes (Ag–Nc)@$CoFe_2O_4$/g–$C_3N_4$ nanostructures using the polyol method and their employment as electrocatalysts for HER and OER in alkaline media.

## 2. Materials and Methods

### *2.1. Materials and Synthesis*

Melamine (99%), Fe(II) acetylacetonaye ($C_{15}H_{24}FeO_6$, 99%, labeled as No. 1), Co(II) acetylacetonate ($C_{10}H_{14}CoO_4$, 99%, labeled as No. 2), $AgNO_3$ (99%), methanol ($CH_3OH$, 99%), tetraethylene glycol (TEG, $HO(CH_2CH_2O)_3CH_2CH_2OH$, 99%), 1,5-pentanediol, potasium hydroxide (KOH, 98.8%) were used for the synthesis.

#### 2.1.1. Synthesis of g–$C_3N_4$

At first, the g–C3N4 was prepared using thermal annealing of melamine at a temperature of 520 oC for 4 h. The precursor was placed in a closed high-alumina crucible and heated to temperature with a rate of 5 °C/min. After the synthesis, it was ground into a fine powder.

Preprints (www.preprints.org) | NOT PEER-REVIEWED | Posted: 1 August 2023 doi:10.20944/preprints202308.0027.v1



The XRD pattern of as-prepared g–$C_3N_4$ exhibited a typical pattern, with two pronounced peaks centered approximately at 13.2° and 27.3° (Figure 2), which may be assigned to the (100) and (002) planes of the trigonal N bond of tri-s-triazine and the layered packing of conjugated aromatic units in g–$C_3N_4$, respectively [34–36].

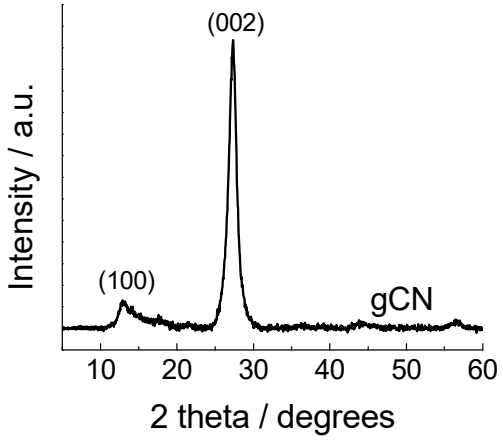


**Figure 2.** XRD patterns for g–$C_3N_4$.

2.1.2. Synthesis of $CoFe_2O_4$/g–$C_3N_4$ nanoparticles using the polyol method

0.112 mmol of reagent No. 1 ($C_{15}H_{24}FeO_6$) and 0.056 mmol of reagent No. 2 ($C_{10}H_{14}CoO_4$) were dissolved in 8 ml of TEG under ultrasonication. Then, 0.041 mmol of synthesized g–$C_3N_4$ was added to the reaction mixture. Scheme of reaction mixture is shown in Figure 3.

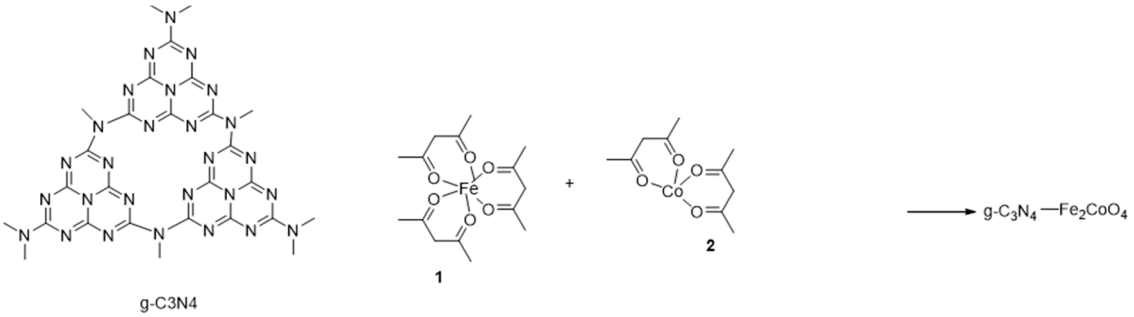


**Figure 3.** Scheme of synthesis of $CoFe_2O_4$/g–$C_3N_4$.

The resultant mixture was kept in a microwave reactor „Monowave 300“ (Anton Paar). Synthesis was carried out according to the following protocol: the temperature was increased up to 180 °C in 2 min followed by the temperature increase up to 270 °C in 3 min. Then, the synthesis was carried out at 270 °C for 58 min. The reaction mixture during synthesis was stirring with a magnetic stirrer. The obtained product was washed 4 times with methanol, separating the particles with a neodymium magnet. The final colloid of nanoparticles was diluted with methanol to 1.5 ml.

2.1.3. Synthesis of Ag nanocubes

Ag nanocubes were synthesized according to the procedure described in [37]. Briefly, 2.94 mmol of $AgNO_3$ and 0.0064 µmol of $CuCl_2$ were dissolved in 12.5 ml of 1,5-pentanediol. In a separate flask, 2.215 mmol of PVP was dissolved in 12.5 ml of 1,5-pentanediol. Using a temperature-controlled silicone oil bath, a reaction flask containing 20 ml of 1,5-pentanediol was heated up to 175 °C and maintained for 10 min. Then the two precursor solutions were injected into the hot reaction flak at different rates: 0.5 mL of $AgNO_3$ solution every minute and 0.25 mL of the PVP solution every 30 s. $AgNO_3$ is poured 7 times, PVP - 14. The reaction was stopped by simply removing it from the heat source and waiting for it to cool down. Additionally, methanol was added for dilution. Particles were deposited by centrifugation at 8000 rpm for 8 min. After deposition, the final product was washed

Preprints (www.preprints.org) | NOT PEER-REVIEWED | Posted: 1 August 2023 doi:10.20944/preprints202308.0027.v1



with methanol 3 times by mixing the particles in an ultrasonic bath. The resulting nanoparticle colloid was diluted with methanol to 3 ml.

2.1.4. $Ag/CoFe_2O_4/g–C_3N_4$

To obtain $Ag/CoFe_2O_4/g–C_3N_4$, 250 µL of prepared $CoFe_2O_4/g–C_3N_4$ solution was mixed with 100 µL of silver colloidal solution and kept for at least 1 day with occasional stirring in UG.

*2.3. Electrochemical Measurements*

The performance of synthesized samples was evaluated using a potentiostat/galvanostat PGSTAT100 (Metrohm Autolab B. V., Utrecht, The Netherlands). Standard three-electrode cell was used, where the working electrode was a glassy carbon (GC) electrode modified with the synthesized samples. A geometric surface area of GC electrode was 0.196 cm2. An Ag/AgCl (3 M KCl) and GC road were employed as the reference and counter electrodes, respectively. Linear sweep voltammograms (LSVs) were recorded in a 1 M KOH solution at a scan rate of 2 mV $s^{-1}$. All reported potential values were referred to as "RHE" – reversible hydrogen electrode according to the following Eqn. 1:

$$E_{RHE} = E_{measured} + 0.059 \cdot pH + E_{Ag/AgCl\ (3\ M\ KCl)} \quad (1)$$

where $E_{Ag/AgCl\ (3\ M\ KCl)} = 0.210$ V.

Current densities for HER and OER presented in this paper were normalized to the geometric area of catalysts.

**3. Results**

The electrocatalytic activity of prepared catalysts was investigated for HER and OER in an alkaline medium. The HER polarization curves recorded on the $g–C_3N_4$, $CoFe_2O_4/g–C_3N_4$, and $Ag/CoFe_2O_4/g–C_3N_4$ samples in alkaline media are shown in Figure 3a, whereas data of electrochemical performance of the tested catalysts are given in Table 2.

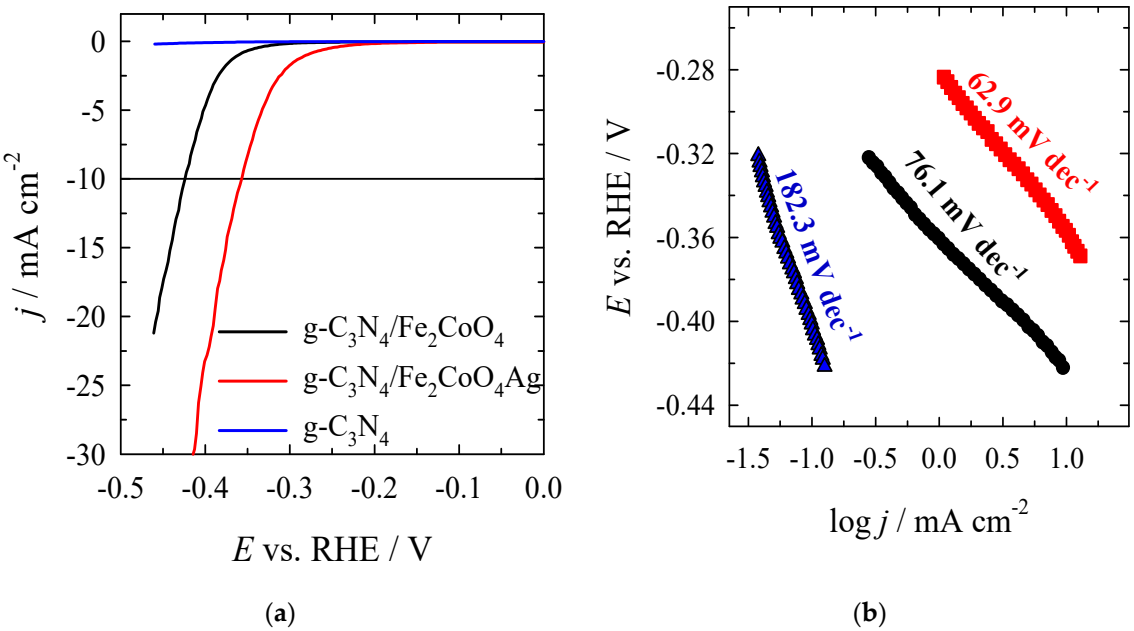


**Figure 2.** (a) HER polarization curves of $g–C_3N_4$, $CoFe_2O_4/g–C_3N_4$, and $Ag/CoFe_2O_4/g–C_3N_4$ catalysts in 1 M KOH solution at a potential scan rate of 2 mV $s^{-1}$; (b) The corresponding Tafel slopes for each catalyst.

Preprints (www.preprints.org) | NOT PEER-REVIEWED | Posted: 1 August 2023 doi:10.20944/preprints202308.0027.v1



**Table 2.** Electrochemical parameters of the investigated materials toward HER in alkaline media.

| Sample | $E_{onset}$, V at $j$ = −0.1 mA cm$^{-2}$ | $\eta_{10}$*, mV | Tafel slope, mV dec$^{-1}$ |
|---|---|---|---|
| g–$C_3N_4$ | −0.40 | – | 182.3 |
| $CoFe_2O_4$/g–$C_3N_4$ | −0.280 | −424.6 | 76.1 |
| Ag/$CoFe_2O_4$/g–$C_3N_4$ | −0.161 | −259.0 | 62.9 |

* Overpotential at 10 mA cm$^{-2}$.

As seen, the lowest onset potential ($E_{onset}$) of −0.161 V for the HER exhibits the Ag/$CoFe_2O_4$/g–$C_3N_4$ sample as compared with $CoFe_2O_4$/g–$C_3N_4$ and pure g–$C_3N_4$ (Table 2). Additionally, the latter catalyst shows the significantly higher current density and the lower overpotential of −259.0 mV for the HER to reach a current density of 10 mA cm$^{-2}$ ($\eta_{10}$) (Figure 3a) as compared to that of $CoFe_2O_4$/g–$C_3N_4$ (−424.6 mV).

The reaction kinetics and mechanism of the as-prepared catalysts can be evaluated on the basis of Tafel slopes determined from the following equation (Eqn. 2) [38]:

$$\eta = b \cdot \log j/j0 \quad (2)$$

η is the overpotential, b is the Tafel slope, j is the experimental current density and j0 is the exchange current density. The plot of η versus log *j* represents the Tafel slope. It is widely accepted that HER proceed by either the Volmer–Heyrovsky or Volmer–Tafel mechanisms and in alkaline media it involves three main steps as shown in equations (3) to (5) [30]:

$$* + H_2O + e^- \rightarrow *H_{ads} + OH^- \quad \text{(Volmer step)} \quad (3)$$

$$*H_{ads} + e^- + H_2O \rightarrow H_2 + OH^- + * \quad \text{(Heyrovsky step)} \quad (4)$$

$$2*H_{ads} \rightarrow H_2 + * \quad \text{(Tafel step)} \quad (5)$$

$H_{ads}$ denotes the $H_2$ adsorbed to the metal sites, where * denotes the metal sites. The theoretical Tafel slopes in the aforementioned reaction steps are 120 mV dec$^{-1}$, 40 mV dec$^{-1}$, and 30 mV dec$^{-1}$, respectively. Figure 3b shows the Tafel slopes of g–$C_3N_4$, $CoFe_2O_4$/g–$C_3N_4$, and Ag/$CoFe_2O_4$/g–$C_3N_4$ samples pointing to the rate-determining step and the likely mechanism associated with electrocatalytic hydrogen generation. The Ag/$CoFe_2O_4$/g–$C_3N_4$ sample was found to have the lowest Tafel slope of 62.9 mV dec$^{-1}$ compared to $CoFe_2O_4$/g–$C_3N_4$ (79.1 mV dec$^{-1}$), and g–$C_3N_4$ (182.3 mV dec$^{-1}$). This predicts the favorable HER kinetics following the Volmer-Heyrovsky mechanism on the $CoFe_2O_4$/g–$C_3N_4$, and Ag/CoFe2O4/g–C3N4.

Among the investigated catalysts, the lower Eonset of −0.161 V, a small overpotential of −259 mV at 10 mA cm$^{-2}$, and a low Tafel slope of 62.9 mV dec$^{-1}$ Ag/$CoFe_2O_4$/g–$C_3N_4$ indicate that the addition of silver nanocubes to $CoFe_2O_4$/g–$C_3N_4$ increases the activity for HER.

### *3.3. Investigation of Electrocatalysts Activity for OER*

The performance of catalysts for OER was further evaluated. Figure 4a,b presents the OER polarization curves and the corresponding Tafel slopes recorded on the g–$C_3N_4$, $CoFe_2O_4$/g–$C_3N_4$, and Ag/$CoFe_2O_4$/g–$C_3N_4$ at a slow scan rate of 2 mV s$^{-1}$ in 1 M KOH solution. The summarized data are also given in Table 3.

**Table 3.** Electrochemical parameters of the investigated catalysts toward OER in alkaline media.

| Catalysts | $E_{onset}$, V at $j$ = 0.1 mA cm$^{-2}$ | $\eta_{onset}$, mV | $E$, V at $j$ = 10 mA cm$^{-2}$ | $\eta_{10}$*, mV | Tafel slope, mV dec$^{-1}$ |
|---|---|---|---|---|---|
| g–$C_3N_4$ | 1.6404 | 410.4 | – | – | 139.9 |
| $CoFe_2O_4$/g–$C_3N_4$ | 1.5056 | 275.6 | 1.6127 | 382.7 | 52.3 |
| Ag/$CoFe_2O_4$/g–$C_3N_4$ | 1.4855 | 255.5 | 1.6000 | 370.2 | 48.1 |

Preprints (www.preprints.org) | NOT PEER-REVIEWED | Posted: 1 August 2023 doi:10.20944/preprints202308.0027.v1



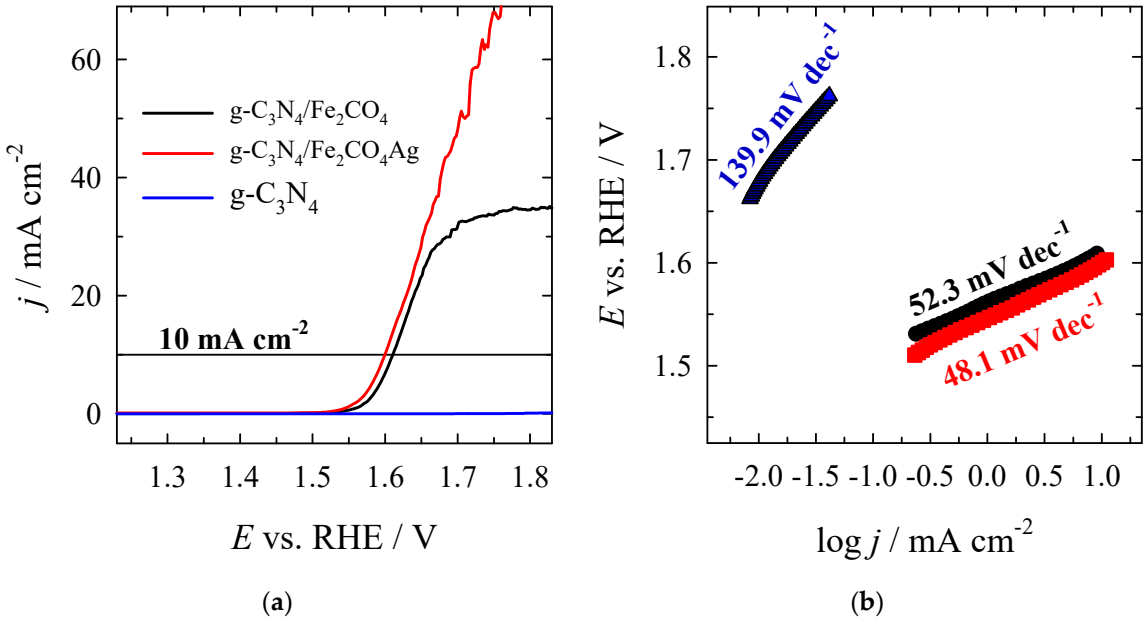


**Figure 4.** (a) OER polarization curves of g–$C_3N_4$, $CoFe_2O_4$/g–$C_3N_4$, and Ag/$CoFe_2O_4$/g–$C_3N_4$ catalysts in 1 M KOH solution at a potential scan rate of 2 mV $s_{-1}$; (b) The corresponding Tafel slopes for each catalyst.

Notably, pure g–$C_3N_4$ shows poor OER activity with a low current density, even at high overpotential. On the contrary, $CoFe_2O_4$/g–$C_3N_4$ and Ag/$CoFe_2O_4$/g–$C_3N_4$ gave much higher current densities and lower overpotentials compared to g–$C_3N_4$, meaning the significant improvement for OER catalytic activity. $E_{onset}$ values were found in a gradual increasing order, as follows: Ag/$CoFe_2O_4$/g–$C_3N_4$ (1.4855 V) < $CoFe_2O_4$/g–$C_3N_4$ (1.5056 V) < g–$C_3N_4$ (1.6404 V) with overpotential values of 255.5, 275.6, and 410.4 mV, respectively (Table 3). Overpotentials to reach the current density of 10 mA·$cm^{-2}$ were found as 370.2 and and 382.7 mV for Ag/$CoFe_2O_4$/g–$C_3N_4$ and $CoFe_2O_4$/g–$C_3N_4$, respectively (Table 3). The Tafel slope of Ag/$CoFe_2O_4$/g–$C_3N_4$ (48.1 mV $dec^{-1}$) is lower than those of $CoFe_2O_4$ and g–$C_3N_4$ (Figure 3b, Table 3), indicating the better catalytic activity for the OER. A 4$e^-$ mechanism is widely accepted for the OER .process. The steps of the reaction in an alka-line media can be represented by Eqns. 6–9 [30,39,40]:

$$* + OH^- \rightarrow e^- + OH^* \quad (6)$$

$$OH^- + OH^* \rightarrow e^- + O^* + H_2O \quad (7)$$

$$OH^- + O^* \rightarrow e^- + OOH^* \quad (8)$$

$$OH^- + OOH^* \rightarrow H_2O + {}^* + e^- + O_2 \quad (9)$$

where * denotes the electrocatalyst's adsorption site, similarly, during OER, the adsorbed intermediates are OH*, O*, and OOH*. The first step of the OER process denoted by equation (6) is the electrosorption of $OH^-$ onto the active sites of the catalyst's surface. Higher oxidation state metal species are more susceptible to adsorb $OH^-$, accelerate the multielec-tron transportation process and, hence, can therefore enhance the OER process [39,40]. The catalytic activity of the $CoFe_2O_4$/g–$C_3N_4$ and Ag/$CoFe_2O_4$/g–$C_3N_4$ materials is also compared with previously reported works and is presented in Table 4. These overpotentials are comparable to those previously reported for state-of-the-art non-precious metal catalysts for water splitting in an alkaline medium.

**Table 4.** Electrochemical parameters of different Co-based gCN catalysts for HER and OER in alkaline media.

| Catalyst | Electrolyte | HER | | OER | | Ref. |
|---|---|---|---|---|---|---|
| | | $\eta_{10}$*, mV | Tafel slope, mV dec$^{-1}$ | $\eta_{10}$*, mV | Tafel slope, mV dec$^{-1}$ | |
| $CoFe_2O_4$/g–$C_3N_4$ | 1 M KOH | 424.6 | 76.1 | 382.7 | 52.3 | This study |
| Ag/$CoFe_2O_4$/g–$C_3N_4$ | 1 M KOH | 259.0 | 62.9 | 370.2 | 48.1 | This study |
| $CoFe_2O_4$/gCN/NGQDs | 1 M KOH | 287 | 96 | 445 | 69 | [30] |
| $Co_2FeO_4$@rGO (CFG-10) | 1 M KOH | 320 | 48 | 240 at 20mA cm$^{-2}$ | 51 | [6] |
| $Co_2FeO_4$@PdO | 1 M KOH | 269 | 49 | 259 at 20mA cm$^{-2}$ | 59 | [41] |
| $CoNi_2S_4$/gCN | 1 M KOH | 160 | 90.76 | 310 at 30mA cm$^{-2}$ | 49.86 | [42] |
| Co-SCN/RGO | 1 M KOH | 150 | 94 | 250 | 96 | [43] |
| $Co_3O_4$/g–$C_3N_4$ | 1 M KOH | 313 | 169 | 315 | 67 | [44] |
| $Co_3O_4MoO_3$/g-$C_3N_4$ | 1 M KOH | 125 | 94 | 206 | 60 | [44] |

* Overpotential at 10 mA cm$^{-2}$.

The above results demonstrate that $CoFe_2O_4$/g–$C_3N_4$ and Ag/$CoFe_2O_4$/g–$C_3N_4$ materials could act as a bifunctional catalyst due to the notable performance towards HER and OER and for total water splitting in practical applications is a promising alternative to noble metal-based electrocatalysts.

## 4. Conclusions

In this study, we reported the synthesis of cobalt ferrite oxide ($CoFe_2O_4$)@g–$C_3N_4$ and silver nanocubes@$CoFe_2O_4$/g–$C_3N_4$ nanostructures using the polyol method and their employment as electrocatalysts for HER and OER in alkaline media. It was found that the Ag/$CoFe_2O_4$/g–$C_3N_4$ shows the highest current density and gives the lowest overpotential of −259 mV for HER to reach a current density of 10 mA cm$^{-2}$ in 1 M KOH. Overpotentials to reach the current density of 10 mA·cm$^{-2}$ for OER are 370.2 mV and 382.7 mV for Ag/$CoFe_2O_4$/g–$C_3N_4$ and $CoFe_2O_4$/g–$C_3N_4$, respectively. The above results demonstrate that $CoFe_2O_4$/g–$C_3N_4$ and Ag/$CoFe_2O_4$/g–$C_3N_4$ materials could act as a bifunctional catalyst due to the notable performance towards HER and OER and for total water splitting in practical applications is a promising alternative to noble metal-based electrocatalysts.

**Author Contributions:** Conceptualization, A.Z., E.N., and L.T.-T.; methodology, R.L. and O.E.-L.; validation, R.L. and O.E.-L., data curation, D.S. and A.Z.; writing—original draft preparation, A.Z., D.S., R.L. and L.T.-T.; writing—review and editing, E.N., D.S., and A.Z.; supervision, A.Z. and E.N.; project administration, E.N. All authors have read and agreed to the published version of the manuscript.

**Funding:** This project has receive funding from European Social Fund (project No. 09.3.3-LMT-K-712-23-0188) under a grant agreement with the Research Council of Lithuania (LMTLT).

**Data Availability Statement:** Not applicable.

**Conflicts of Interest:** The authors declare no conflict of interest.

## References

1. Y. Gong, J. Yao, P. Wang, Z. Li, H. Zhou, C. Xu. Perspective of hydrogen energy and recent progress in electrocatalytic water splitting. *Chin. J. Chem. Engineer.* **2022**, *43*, 282–296, https://doi.org/10.1016/j.cjche.2022.02.010
2. Z.-Y. Yu, Y. Duan, X.-Y. Feng, X.g Yu, M.-R. Gao, S.-H. Yu. Clean and affordable hydrogen fuel from alkaline water splitting: past, recent progress, and future prospects. *Adv. Mater.* **2021**, 2007100, https://doi.org/10.1002/adma.202007100
3. Y. Yao, X. Gao, X. Meng. Recent advances on electrocatalytic and photocatalytic seawater splitting for hydrogen evolution. *Int. J. Hydrogen Energy* **2021**, 469087–9100, https://doi.org/10.1016/j.ijhydene.2020.12.212

4. L.G. Li, P.T. Wang, Q. Shao, X.Q. Huang. Metallic nanostructures with low dimensionality for electrochemical water splitting. *Chem. Soc. Rev.* **2020**, *49(10)*, 3072–3106, https://doi.org/10.1039/D0CS00013B
5. B. You, Y. Sun. Innovative strategies for electrocatalytic water splitting. *Acc. Chem. Res.* **2018**, *51(7)*, 1571–1580, https://doi.org/10.1021/acs.accounts.8b00002
6. A. Hanan, D. Shu, U. Aftab, D. Cao, A. J. Laghari, M. Y. Solangi, M. I. Abro, A. Nafady, B. Vigolo, A. Tahira, Z. H. Ibupoto. $Co_2FeO_4$@rGO composite: Towards trifunctional water splitting in alkaline media. Int. J. Hydrogen Energy 47 (2022) 33919-33937.
7. H. Sun, J. Meng, L. Jiao, et al. *Inorg. Chem. Front*. **2018**, *5*, 760, 10.1039/c8qi00044a.
8. A. Thomas, A. Fischer, F. Goettmann, M. Antonietti, J.-O. Müller, R. Schlügl, J. M. Carlsson. Graphitic carbon nitride materials: variation of structure and morphology and their use as metal-free catalysts. *J. Mater. Chem*. **2008**, *18*, 4893-4908. DOI: 10.1039/b800274f
9. M. Kim, S. Hwang, J.S. Yu. Novel ordered nanoporous graphitic $C_3N_4$ as a support for Pt–Ru anode catalyst in direct methanol fuel cell. *J. Mater. Chem*. **2007**, *17*, 1656–1659.
10. M. Groenewolt, M. Antonietti. Synthesis of g-$C_3N_4$ nanoparticles in mesoporous silica host matrices. Adv. Mater. **2005**, *17*, 1789–1792.
11. S.C. Yan, Z.S. Li, Z.G. Zou. Photodegradation performance of g-$C_3N_4$ fabricated by directly heating melamine. Langmuir **2009**, *25*, 10397–10401.
12. X.F. Li, J. Zhang, L.H. Shen, et al. Preparation and characterization of graphitic carbon nitride through pyrolysis of melamine. *Appl. Phys. A* **2009**, 94, 387–392.
13. Q. Gu, Z. Gao, H. Zhao, Z. Lou, Y. Liao, C. Xue. Temperature-controlled morphology evolution of graphitic carbon nitride nanostructures and their photocatalytic activities under visible light. *RSC Adv*. **2015**, *5*, 49317–49325, https://doi.org/10.1039/C5RA07284K
14. Li, L. Zhou, S. Guo. Noble metal-free electrocatalytic materials for water splitting in alkaline electrolyte. *EnergyChem* **2021**, *3*, 100053, https://doi.org/10.1016/j.enchem.2021.100053
15. S. Li, E.Li, X. An, X. Hao,Z. Jiange, G. Guan. Transition metal-based catalysts for electrochemical water splitting at high current density: current status and perspectives. *Nanoscale* **2021**, *13*, 12788-127817, https://doi.org/10.1039/D1NR02592A
16. H. Wu, C. Feng, L. Zhang, J. Zhang, D.P. Wilkinson. Non-noble metal electrocatalysts for the hydrogen evolution rea-ction in water electrolysis. *Electrochem. Energy Rev*. 2021, *4*, 473–507, https://doi.org/10.1007/s41918-020-00086-z
17. A.H. Al-Naggar, N.M. Shinde, J.-S. Kim, R.S. Mane. Water splitting performance of metal and non-metal-doped transi-tion metal oxide electrocatalysts. *Coord. Chem. Rev*. **2023**, *474*, 214864, https://doi.org/10.1016/j.ccr.2022.214864
18. Z. Chen, W. Wei, B.-J. N. Cost-effective catalysts for renewable hydrogel production via electrochemical water splitting: Recent advances. Curr. Opin. Green Sustain. Chem. **2021**, *27*, 100398, https://doi.org/10.1016/j.cogsc.2020.100398
19. P. Du, R. Eisenberg. Catalysts made of earth-abundant elements (Co, Ni, Fe) for water splitting: recent progress and future challenges. *Energy Environ. Sci*. **2012**, *5*, 6012–6021, https://doi.org/10.1039/C2EE03250C
20. X. Cao, T. Wang, L. Jiao. Transition-metal (Fe, Co, and Ni)-based nanofiber electrocatalysts for water splitting. *Adv. Fi-ber Mater*. **2021**, *3*, 210–228, https://doi.org/10.1007/s42765-021-00065-z
21. L. Han, S. Dong., E. Wang. Transition-metal (Co, Ni, and Fe)-based electrocatalysts for the water oxidation reaction. *Adv. Mater*. **2016**, *28*, 9266–9291, https://doi.org/10.1002/adma.201602270
22. D. Liu, H. Ai, M. Chen, P. Zhou, B. Li, et al. Multi-phase heterostructure of CoNiP/$Co_xP$ for enhanced hydrogel evolution under alkaline and seawater conditions by promoting $H_2O$ dissociation. *Small* **2021**, *17*, 2007557, https://doi.org/10.1002/smll.202007557
23. H. Jung, A. Ma, S. A. Abbas, H. Y. Kim, H. R. Choe, S. Y. Jo, K. M. Nam. A new synthetic approach to cobalt oxides: Designed phase transformation for electrochemical water splitting. *Chem. Engineer. J.* **2021**, *415*, 127958, https://doi.org/10.1016/j.cej.2020.127958
24. M. Duraivel, S. Nagappan, K. H. Park, K. Prabakar. Hierarchical 3D flower like cobalt hydroxide as an efficient bifunctional electrocatalyst for water splitting. *Electrochim. Acta* **2022**, *411*, 140071, https://doi.org/10.1016/j.electacta.2022.140071
25. Z. Xue, J. Kang, D. Guo, C. Zhu, C. Li, X. Zhang, Y. Chen. Self-supported cobalt nitride porous nanowire arrays as bi-functional electrocatalyst for overall water splitting. Electrochim. Acta **2018**, *273*, 229–238, https://doi.org/10.1016/j.electacta.2018.04.056
26. H. Zou, G. Li, L. Duan, Z. Kou, J. Wang. In situ coupled amorphous cobalt nitride with nitrogen-doped graphene aerogel as a trifunctional electrocatalyst towards Zn-air battery deriven full water splitting. *Appl. Catal. B: Environm*. **2019**, *259*, 118100, https://doi.org/10.1016/j.apcatb.2019.118100
27. H. Bian, T. Chen, Z. Chen, J. Liu, Z. Li, P. Du, B. Zhou, X. Zeng, J. Tang, C. Liu. One-step synthesis of mesoporous cobalt sulfides ($CoS_x$) on the metal substrate as an efficient bifunctional electrode for overall water splitting. Electrochim. Acta **2021**, *389*, 138786, https://doi.org/10.1016/j.electacta.2021.138786

28. Y. Wu, F.Wang, N. Ke, B. Dong, A. Huang, C. Tan, L. Yin, X. Xu, L. Hao, Y. Xian, S. Agathopoulos, Self-supported co-balt/cobalt selenide heterojunction for highly efficient overall water splitting. *J. Alloys Compd*. **2022**, *925*, 166683, https://doi.org/10.1016/j.jallcom.2022.166683
29. Q. Wang, R. He, F. Yang, X. Tian, H. Sui, L. Feng. An overview of heteroatom doped cobalt phosphide for efficient elec-trochemical water splitting. *Chem. Engineer. J.* **2023**, *456*, 141056, https://doi.org/10.1016/j.cej.2022.141056
30. B Shalini Reghunath, Sruthi Rajasekaran, Sunava Devi K R, Dephan Pinheiro, Jadan Resnik Jaleel UC. N-doped graphene quantum dots incorporated cobalt ferrite/graphitic carbon nitride ternary composite for electrochemical overall water splitting. *Int. J. Hydrogen Energy* **2023**, *48*, 2906–2919, https://doi.org/10.1016/j.ijhydene.2022.10.169
31. F. T. Haase, A. Rabe, F.-P. Schmidt, A. Herzog, H. S. Jeon, W. Frandsen, P.V. Narangoda, I. Spanos, K. F. Ortega, J. Timoshenko, T. Lunkenbein, M. Behrens, A. Bergmann, R. Schlögl, B. R. Cuenya. Role of nanoscale inhomogeneities in $Co_2FeO_4$ catalysts during the oxygen evolution reaction. J. Am. Chem. Soc. 144 (2022) 12007-12019.
32. C. Huang, P. Qin, Y. Luo, Q. Ruan, L. Liu, Y. Wu, Q. Li , Y. Xu, R. Liu, P.K. Chu. Recent progress and perspective of cobalt-based catalysts for water splitting: design and nanoarchitectonics. *Mat. Today Energy* 2022, 23, 10091, https://doi.org/10.1016/j.mtener.2021.100911
33. W. Zhang, L. Cui, J. Liu. Recent advances in cobalt-based electrocatalysts for hydrogen and oxygen evolution reactions. *J. Alloys Compd*. **2020**, *821*, 153542, https://doi.org/10.1016/j.jallcom.2019.153542
34. Q. Gu, Z. Gao, H. Zhao, Z. Lou, Y. Liao, C. Xue. Temperature-controlled morphology evolution of graphitic carbon nitride nanostructures and their photocatalytic activities under visible light. RSC Adv. **2015**, *5*, 49317–49325, https://doi.org/10.1039/C5RA07284K
35. C. Hu, Y.-C. Chu, M-S Wang, W. Xiao-Han. Rapid synthesis of g-$C_3N_4$ spheres using microwave-assisted solvothermal method for enhanced photocatalytic activity. *J. Photochem. Photobiol. A: Chem*. **2017**, *348*, 8–17, http://dx.doi.org/10.1016/j.jphotochem.2017.08.006
36. H. Chen, Y. Fan, H. Xu, D. Cui, C. Xue, W. Zhang. A facile and green microwave hydrothermal method for fabricating g-$C_3N_4$ nanosheets with improved hydrogen evolution performance. *J. Alloys Compn*. 2021, *863*, 158448, https://doi.org/10.1016/j.jallcom.2020.158448
37. Tao, A.; Sinsermsuksakul, P.; Yang, P. Polyhedral silver nanocrystals with distinct scattering signatures. *Angew. Chem*., Int. Ed. **2006**, *45*, 4597−4601.
38. G. X. Zhu, T. L. Lu, L. Han, Y. Z. Zhan. Graphitic carbon nitride (g–$C_3N_4$) as an efficient metal-free Fenton-like catalyst for degrading organic pollutants: the overlooked non-photocatalytic activity. *Water Sci. Technol*. **2020**, *81*, 518–528, https://doi.org/10.2166/wst.2020.129
39. H. Bian, T. Chen, Z. Chen, J. Liu, Z. Li, P. Du, B. Zhou, X. Zeng, J. Tang, C. Liu. One-step synthesis of mesoporous cobalt sulfides (CoSx) on the metal substrate as an efficient bifunctional electrode for overall water splitting. *Electrochim. Acta* **2021**, *389*, 138786, https://doi.org/10.1016/j.electacta.2021.138786
40. M. Plevová, J. Hnát, K. Bouzek. Electrocatalysts for the oxygen evolution reaction in alkaline and neutral media. A comparative review. *J. Power Sources* 2021, *507*, 230072, https://doi.org/10.1016/j.jpowsour.2021.230072
41. A. Hanan, M. N. Lakhan, D. Shu, A. Hussain, M. Ahmed, I. A. Soomro, V. Kumar, D. Cao. An efficient and durable bifunctional electrocatalysts based on PdO and Co2FeO4 for HER and OER. *Int. J. Hydrogen Energy* **2023**, *48*, 19494-19508.
42. R. Zahra, E. Pervaiz, M.M. Baig, O. Rabi. Three-dimensional hierarchical flowers-like cobalt-nickel sulfide constructed on graphitic carbon nitride: bifunctional non-noble electrocatalyst for overall water splitting. *Electrochim. Acta* **2022**, *418*, 140346, https://doi.org/10.1016/j.electacta.2022.140346
43. W.-K. Jo, S. Moru, S. Tonda. Cobalt-coordinated sulfur-doped graphitic carbon nitride on reduced graphene oxide: an efficient metal−(N,S)−C-class bifunctional electrocatalyst for overall water splitting in alkaline media. *ACS Sustain. Chem. Eng*. **2019**, *7*, 15373−15384, DOI: 10.1021/acssuschemeng.9b02705
44. Ahmed, R. Biswas, R. A. Patil, K. K. Halder, H. Singh, B. Banerjee, B. Kumar, Y.-R. Ma, K. K. Haldar. Graphitic carbon nitride composites with $MoO_3$-decorated $Co_3O_4$ nanorods as catalysts for oxygen and hydrogen evolution. *ACS Appl. Nano Mat*. **2021**, *4*, 12672−12681, https://doi.org/10.1021/acsanm.1c03238